A New Geophysical Sensor: Ultra-Lightweight Electromagnetic Array

Michele Maxson[1], Maximilian Orman-Kollmar, Dr. Fridon Shubitidze
Dartmouth College, Hanover, NH
UNITED STATES

Randall Reynolds, David Lozano, Brian Quinn, Dr. Benjamin Barrowes
[1](Also) U.S. Army ERDC Cold Regions Research and Engineering Laboratory, Hanover, NH
UNITED STATES

Mikheil Prishvin
Subsurface Sensing Technologies, Tbilisi
GEORGIA

michele.l.maxson@usace.army.mil

ABSTRACT

This paper presents the first time a fully integrated and advanced electromagnetic induction (EMI) sensor has been deployed on an unmanned aerial system (UAS) together with signals processing approaches for the purpose of unexploded ordnance (UXO) detection and classification. Existing solutions can detect and classify UXO, but they are large and cannot be deployed in challenging environments. This new ultra-lightweight electromagnetic array (ULEMA) sensor is light enough to be mounted on a UAS, making it deployable in rocky or marshy environments, as well as keeping human operators out of the field with live UXO. Other variants of this ULEMA sensor are handheld and robot-mounted, aimed at different environments and deployment challenges. This paper discusses the performance of the UAS-borne variant.

1.0 INTRODUCTION

Unexploded Ordnance (UXO) is a global problem that requires remediation. Traditional time domain Electromagnetic Induction (EMI) sensors for UXO detection utilize a human operated vehicle or human powered cart for data collection. These advanced geophysical sensors, such as MetalMapper 2x2, TEMTADS, APEX and ULTRATEM, can detect, locate, classify, and discriminate munitions to allow for faster and safer remediation of UXO [2]-[11]. Operating these sensors in rough terrain is challenging since they are heavy and require a human operated cart or vehicle to push or pull the sensor array over the munitions. Vehicles or human powered carts cannot traverse rough terrain easily which limits data collection to flat open areas or increases the difficulty of data collection. Furthermore, rough terrain decreases the signal to noise ratio due to added vibrations and increased movement of the sensor array. As a result, targets may not be detected or may be incorrectly classified. Additionally, human operation of sensors in UXO contaminated areas is dangerous due to the potential for unwanted detonation and chemical hazards, particularly in active war zones. The problem that UXO creates globally is not diminishing with time. For example, according to world bank's initial estimates at the end of December 2022, roughly 64-thousand square miles of Ukrainian territory have been impacted and contaminated with UXO over the last year of war [1]

Mounting EMI sensors to an unmanned aerial system (UAS) could help mitigate these limitations while increasing safety and reducing operational costs. Signal to noise ratio (SNR) degradation caused by platform motion over rough terrain would be mitigated because the drone should encounter less unexpected jarring of the system and more consistent overall vibrations. The UAS would also be controlled remotely, removing the human from potential contact with a UXO. However, several challenges must be overcome before EMI sensors can be successfully deployed on a UAS. The two primary challenges include weight limitations and EMI interference from the UAS platform.

The main goal of this paper is to demonstrate the development and deployment of a UAS mountable time domain EMI sensor, the Ultra-lightweight Electromagnetic Array (ULEMA), developed by the Thayer Engineering School at Dartmouth College and the Cold Region Research and Engineering Laboratory (CRREL). ULEMA is light enough to deploy in handheld and drone applications, the total weight of the platform varies slightly depending on the deployment method. We will show results from deployments of ULEMA on a UAS platform in this paper. The first version of the ULEMA was the ULEMA-H(handheld) [2]. The second version of the ULEMA is the ULEMA-A(airborne), discussed in this paper. ULEMA-A has been calibrated and preliminary testing was conducted in previous years which lead to the design which is seen in this report [3], [4].

The paper is organized as: first the hardware, the sensor development progressions and sensor's geometry are discussed, then experimental designs, sensor function test, and test flight are highlighted; third, forward and inverse EMI models described briefly, and finally experimental data and classification results are presented.

2.0 HARDWARE

The Ultralight Electromagnetic Array (ULEMA) is a new geophysical sensor intended to improve the process for finding and discriminating subsurface UXO. The sensor consists of four transmitter coils and four triaxial receiver cubes. Three of the transmitter coils are oriented to form a triangle, with the fourth transmitter being wrapped around the other three (Figure 1). The triaxial receiver cubes are oriented in the three Cartesian directions and are located inside the transmitter coils. Each of the transmitter coils gets a 10 A, 50 % duty cycle current pulse sent in on-off cycles of 8.33 msec. The current in the transmitter coils creates a primary magnetic field which interacts with conductive material. As a result of this interaction, highly conductive materials respond with inducing eddy currents in the conductive object. The eddy currents create a secondary magnetic field which is sensed by the receiver cubes. The received signal is sent as a voltage value to an oscilloscope. From there it is stored to a file for processing.

To address various environmental scenarios and fast and cost effective UXO clean up needs, the ULEMA system have been developed: the handheld, airborne, and robotic systems (ULEMA-H, ULEMA-A, ULEMA-R). All these systems provide high quality data in dynamic modes, which in return enabled us to achieve UXO target detection and classification in single-operation (Dynamic) mode. For land where physically entering would prove difficult, ULEMA-A would be flown over the area of interrogation on a drone platform. For situations where the ground is more stable, either ULEMA-R or ULEMA-H could be implemented. Using ULEMA-R would be preferable, as this would ensure that human operators are as far removed from the hazardous and potentially explosive environments as possible.

2.1 Sensor Progression

To explain the need for the ULEMA systems, the current methods of detection should be discussed. For the operators on the ground, many of the standard systems are essentially metal detectors, alerting an operator that a conducting object is in the vicinity. As a result, any time an area is flagged for interest, it must be fully excavated and examined. Treating any flag as a potential UXO leads to many hours spent and even more dollars expended. The US Congress and US State Department projects 10 billion dollars to be spent in efforts of UXO and landmine clean-up domestically and globally [2], [3].

Systems, such as the MetalMapper, Man Portable Vector (MPV) and Time-Domain Electromagnetic Multisensor Towed Array Detection System (TEMTADS) have been developed to aid in discrimination between clutter and UXO while in the field [4] – [12]. However, they all have drawbacks that have hindered their widespread adoption in the field. One drawback is their size- the TEMTADS system is 2mx2m, necessitating a vehicle or some other towing system to drag it over the area in question [6]. The MetalMapper system is also approximately 2mx2m and weighs 172kg (380 lb), forcing it to be built into a

wheeled frame [12], [13]. Another drawback, seen in the MPV and MPV-II, is the inability to perform identification in a single pass. Due to its single transmitter design, the operator must perform a complete area interrogation in "dynamic collection mode", then post-process the data [14]. Once areas of interest have been identified, the system is brought back out to the flagged spots and data is re-collected in "cued collection mode" with extra transmitters added on. This two-pass interrogation process takes time, requires multiple data processing stages, and longer periods of the operator being in the field [15].

The ULEMA sensor seeks to remedy the above issues. The first iteration tested was a handheld sensor (ULEMA-H) which is light enough to be carried by a single operator. It can be operated in both cued and dynamic modes. The benefit of ULEMA-H is that the system has multiple transmitters and receivers allowing the system to detect and classify targets in a single pass. This single-pass capability reduces both processing time and time that an operator must spend in the field. The first iteration of ULEMA-H had a total approximate weight of 14lbs. The sensor head and carrying mechanism weighed approximately 8lbs with the electronics being carried on the operator's back [16].

Since the issue of having an operator in the field with live UXO is still prevalent, the next logical step was to design a sensor that could be mounted to a drone-the ULEMA airborne (ULEMA-A) variant. ULEMA-A, mounted to a Harris Carrier Hx8 drone, weighs about 14 lbs, and exhibits the same single-pass functionality as the ULEMA-H.

2.2 Sensor Geometry

The ULEMA sensor geometry is similar between all versions presented, only the scaling is different. To create the primary magnetic signal, a set of four transmitter coils are used. Three of the transmitter coils are arranged in the form of a triangle, each at one of the vertices, and the fourth is wound around the other three to create a transmit coil which is larger than the other three transmitter coils. To detect the secondary magnetic field from conducting objects, a set of triaxial receiver cubes is used. Each cube consists of three individual receiver coils, oriented in the three cartesian directions to capture the spatial shape of the magnetic field. Each cube is centred in one of the transmitter coils. The ability to excite a conductive target from at least three different angles and sense the spatial response from the conductive target from multiple locations allows the system to detect and classify the targets in a single pass.

ULEMA-A weighs a total of 14 pounds and is currently being lifted by a Carrier Hx8, a commercially available UAS from Harris Aerial. The only additional engineering for the UAS to lift the payload is the addition of two carbon fiber cross members which are clamped to the legs of the UAS. The sensor is tethered below the UAS by 10ft cables between the cross members and plastic eyebolts which are connected to the sensor (Figure 2).

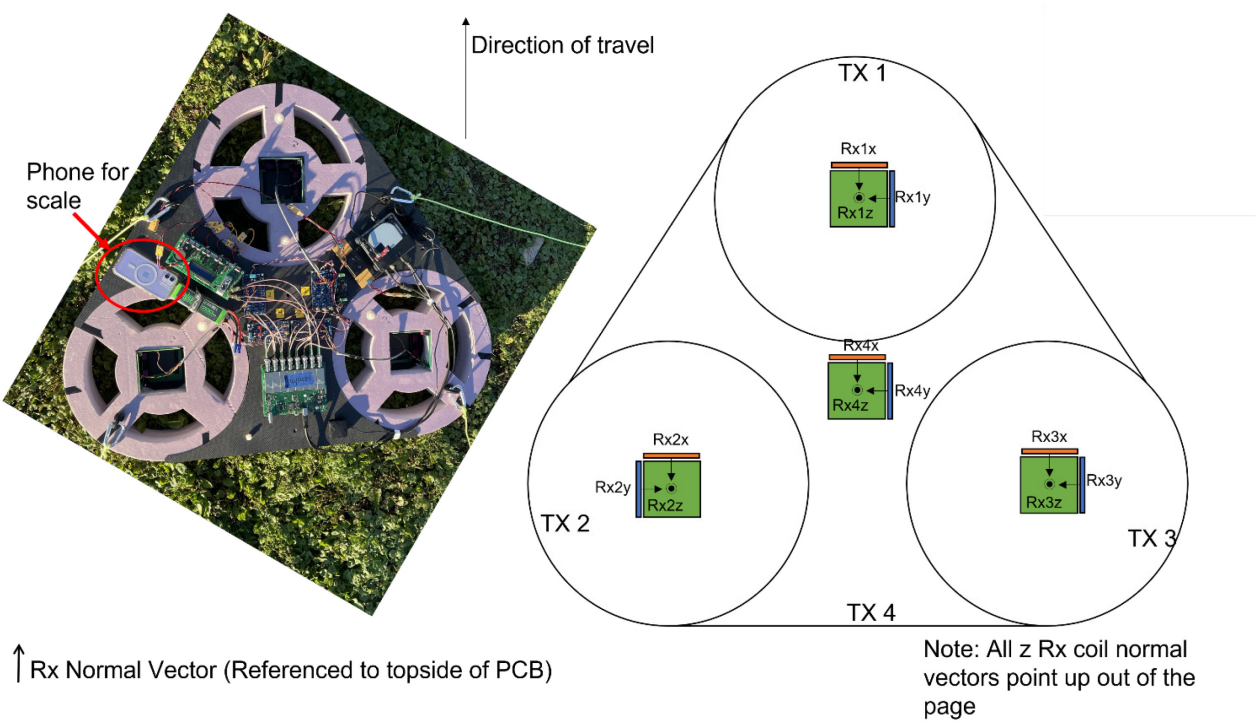

Figure 1: Picture and schematic of ULEMA-A. Phone placed between transmitters 1 and 2 for scale.

Figure 2: ULEMA-A sensor hovering over target.

3.0 EXPERIMENTAL DESIGN

3.1 Data Collection Set Up

ULEMA-A was tested in early February 2023 during the Rapid Airfield Damage Assessment System (RADAS) Fiscal Year '22 Capability Development Demo and Experiment Event sponsored by the United States Air Force Civil Engineering Center at Silver Flag, Florida. The demonstration site was in western Florida, in what is known as the panhandle near Tyndall, AFB. All data collection was conducted on the southern half of the training runway (R-2905B) at the Sliver Flag training site. Holes were blasted to a depth of approximately 1.5m, two (2) large penetrators were placed vertically in camouflet 5 and 7, and one (1) medium penetrator was placed vertically in camouflet 6. All other targets were placed horizontally on the surface of the runway. The targets which were used in this demonstration consisted of large penetrators (mimicking 155s), medium penetrators (mimicking 105s), bomblets, BLU-97s, Rockets, and M82s

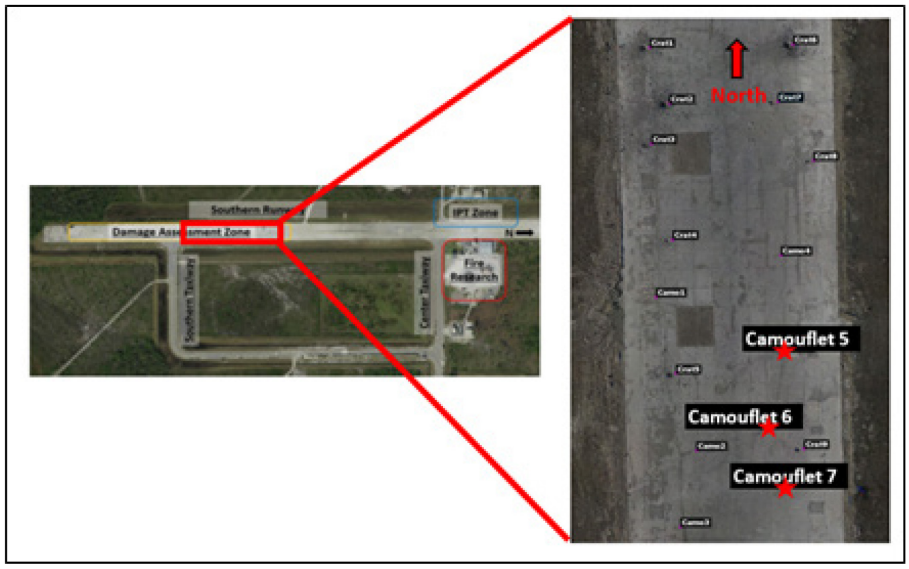

Figure 3: Location of target #2, #3, and #4.

Data was collected in two general steps. First a sensor function test was conducted to verify that the sensor was functioning as anticipated. Second, the sensor was flown to each target to collect data.

3.2 Sensor Function Test

At the beginning of each flight or after the batteries for the sensor were replaced a sensor function test was conducted. This test involved placing a small ISO (schedule 40 steel pipe, 1-inch diameter x 4-inch height) over each receiver. A data set was collected for each of the four locations and the response from the target with respect to each transmitter/receiver combination was verified to have the expected result. The data for each test was than inverted to verify that the expected target and location were accurately solved. This test is run while the sensor is on the ground and the UAS is not running (see Figure 4).

3.3 Test Flights

Currently, GPS has not been integrated into the sensor, but is integrated into the UAS. Therefore, the GPS is used to create a flight plan allowing the UAS to transit to the GPS coordinate in waypoint mode, maintaining the sensor elevation to be several meters from the ground, at a speed of ½ meter per second. Once the UAS traversed to the GPS waypoint, it then lowered to a height approximately 2 meters from the ground. When

the UAS was stationary above the ground, the pilot then took control of the system and lowered the UAS until the sensor was as close to the ground as deemed safe to hover under the manual control of the pilot. The pilot hovered the UAS for a minimum of 20 seconds at the GPS point and then allowed the waypoint navigation software to return the UAS to the transit height and either traversed to the next GPS coordinate or returned to the starting position. It should be noted that the UAS does not take off nor land in waypoint mode, the pilot must be in control during both take-off and landing.

For one (1) of the seven (7) flights a dynamic data collect was conducted. This was done by using GPS coordinates for four (4) targets to create a mission that traversed to all targets, without stopping at a target, at a speed of ½ meter per second. The UAS height above ground was set to a constant 4.15m resulting in a sensor height of approximately 1 meter from the ground. Due to the instability in the GPS vertical accuracy, the height of the sensor may vary $\pm$ 1 m.

To safely take off, the UAS must first take off vertically and only a few feet from the ground, the pilot must than move the UAS laterally over the sensor and then lift the sensor vertically. To land the sensor, the opposite order must be followed. The sensor must first be lowered vertically to the ground and then the UAS must be flown laterally such that the UAS will not land directly on top of the sensor and then the UAS can be landed vertically beside the sensor.

4.0 DATA PROCESSING

4.1 Forward Model

For this preliminary study, data processing was kept to a minimum. To prepare the data for inversion, the first step is to normalize the current in each receiver coil with each corresponding transmitter coil. For example, the currents in receiver 1X, 1Y, and 1Z for each time channel were normalized with respect to the current in the respective time channel in transmitter 1. Then a subset of data was selected after take-off and before landing while the sensor was in the air to use a background data. The average response for each time channel in each transmitter/receiver combination was subtracted from the corresponding transmitter/receiver combinations for the duration of this flight. This both current normalized and removed background from the raw dataset.

To interrogate the targets, an advanced anomaly selection algorithm known as the ortho-normalized volume magnetic source (ONVMS) is implemented. This forward model was developed under the SERDP Project MM-1572 and has been successfully applied for many time-domain electromagnetic induction ground-based systems such as the portable decoupled electromagnetic induction sensor (PEDEMIS), time-domain electromagnetic multi-sensor tower array detection system (TEMTADS) [10], and others at various ESTCP live site demonstrations such as Camp Butner, NC, Camp Sibert, Alabama, USA [15], [17] – [19]. These algorithms have not been used on airborne datasets therefore the preliminary study and demonstration outlined in the paper demonstrates not only the functionality of an airborne sensor, but also the applicability of ground-based inversion algorithms to airborne collected TEM data sets.

ONVMS is a generalized volume dipole model which assumes that a volume of scatterers can be replaced by a set of magnetic dipole sources which are distributed over a volume [17]. These distributed magnetic dipoles then mimic eddy currents which are induced on the target by the sensor which create secondary magnetics fields which are observable by the receiver coils. Since these distributed magnetic dipoles are distributed inside of the target under investigation, the spatial distribution of these responding dipoles creating a “response map” which reveals the locations and orientations of the target(s). The scattered magnetic field at any point which is outside of the target(s) is a superposition of magnetic fields due to a volumetric distribution of magnetic dipole densities:

$$\boldsymbol{H}^{sc}(\boldsymbol{r},p)=\int_V \frac{1}{4\pi R^3}(3\hat{\boldsymbol{R}}\hat{\boldsymbol{R}}-\bar{\bar{\boldsymbol{I}}})\cdot\boldsymbol{m}(\boldsymbol{r}_v',p)dv'=\int_V \bar{\bar{\boldsymbol{G}}}(\boldsymbol{r},\boldsymbol{r}')\cdot\boldsymbol{m}(\boldsymbol{r}_v',p)\ dv' \tag{1}$$

Where $p=\{t,f\}$ is time or frequency, $\hat{\boldsymbol{R}}$ is the unit vector along $\mathbf{R}=\mathbf{r}-\mathbf{r}_v'$, $\mathbf{r}_v'$ is the position of the v'-th infinitesimal dipole in the volume V, $\mathbf{r}$ is the observation point, and $\bar{\bar{\mathbf{I}}}$ and $\bar{\bar{G}}(\mathbf{r},\mathbf{r}')$ are respectively the identity and Green dyads. The induced magnetic dipole moment $\mathbf{m}(\mathbf{r}_{v'},p)$ at point $\mathbf{r}_{v'}$ on the surface is related to the primary field through $\mathbf{m}(\mathbf{r}_{v'},p)=\bar{\bar{\mathbf{M}}}(\mathbf{r}_{v'},p)\cdot\mathbf{H}^{pr}(\mathbf{r}_{v'})$, where $\bar{\bar{\mathbf{M}}}(\mathbf{r}_{v'},p)$ is the symmetric polarizability tensor. The secondary magnetic field at any point can be expanded in a set of orthonormal functions $\bar{\bar{\psi}}_i(\mathbf{r})$ as

$$\mathbf{H}(\mathbf{r})=\sum_{i=1}^{N_v}\bar{\bar{\psi}}_i(\mathbf{R}_i)\cdot\mathbf{b}_i \tag{2}$$

where the expansion coefficients $\mathbf{b}_i$ have been introduced. The $\bar{\bar{\psi}}_i$ functions are linear combinations of dipole Green dyads which are guaranteed to be orthonormal by the Gram–Schmidt process. Based on this normality property, the amplitudes of the tensor elements of $\bar{\bar{\mathbf{M}}}_i(p)$ can be determined without having to solve a linear system of equations. The advantages of the ONVMS are that 1) the couplings between different sections of the target are taken into consideration when the target is comprised of different material types, thicknesses, and shapes, 2) ONVMS avoids the mathematical conundrum of matrix singularity problems in the multi-object case, and 3) ONVMS is stable when used in "noisy" environments therefore works well in real-world applications.

4.2 Inversion Model

It's well known that determining the orientation and location of targets is a non-linear problem and the solution is extracted by solving a forward model, such as the ONVMS, making predictions for the measured quantities and then comparing the misfit between the model and the measured quantity. The method of least squares is used to recover the parameter vector **v** from equation 3. In this case, the parameter vector contains the intrinsic information about the target such as its shape and size. Additionally, the parameter vector also contains the information about the target location and orientation. To be specific, if $\mathbf{d}^{obs}$ is the vector of the measured secondary field, and $\mathbf{F}(\mathbf{v})$ is the solution to the forward model found via ONVMS, the least squares approach uses the criteria:

$$\underset{\mathbf{v}}{\text{minimize}}\quad \phi(\mathbf{v})=\frac{1}{2}\left\|\mathbf{d}^{obs}-\mathbf{F}(\mathbf{v})\right\|^2+\frac{\alpha}{2}\left\|\mathbf{v}-\mathbf{v}_{ref}\right\|^2 \tag{3}$$

Where the regularization of the parameter α accounts for uncertainties caused by the sensor, any measurement error, and additionally background noise. The last term of the right-hand side of equation 3 will determine how close we want the final solution to be to the referenced model $\mathbf{v}_{ref}$. In creating the reference model $\mathbf{v}_{ref}$, priori information such as the global location of the sensor and the spatial behaviour of its primary field can be considered when determining the inversion procedure.

To classify the targets, the ONVMS model provides at least three total time dependent ONVMS parameters which are used in the classification process.

5.0 RESULTS

5.1 Sensor Function Test

To validate that both the sensor is functioning and that the inversion algorithms will correctly classify the target, a full inversion was conducted for the small iso over each of the four receiver cubes before each flight and after batteries were replaced between flights. The resulting polarizability curves from this sensor function test performed on the third day for the first sensor function test are seen in Figure 4 below and the predicted locations are seen in Table 1 below. Only one set of results for the sensor function test are reported in this paper since all sensor function test presented similar data showing that both the sensor and the inversion algorithms are functioning.

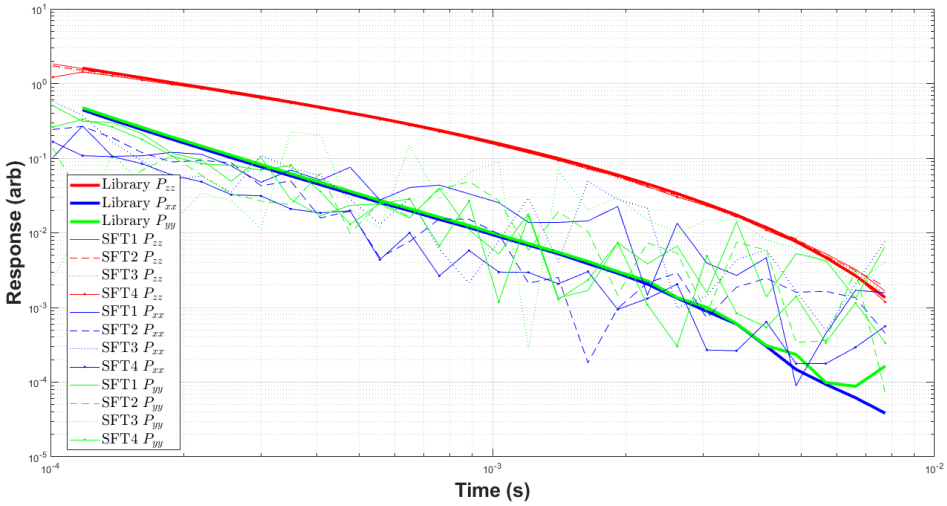

Figure 4: Results for sensor function test for the third day, first sensor function test. Library data is small ISO.

Table 1: True coordinates, inverted (predicted) coordinates, and the absolute difference for the inverted sensor function test.

	True X (cm)	True Y (cm)	True Z (cm)	Pred. X (cm)	Pred.Y (cm)	Pred. Z (cm)	Diff. X (cm)	Diff Y (cm)	Diff Z (cm)
Receiver 1	29.6	0.2	25.00	30.74	-0.91	24.97	**1.14**	**1.11**	**0.03**
Receiver 2	-18.57	34.48	25.00	-20.88	32.54	22.40	**2.31**	**1.94**	**2.60**
Receiver 3	-18.56	-34.09	25.00	-19.95	-35.08	24.31	**1.39**	**0.99**	**0.69**
Receiver 4	0.00	0.00	23.00	2.69	-2.46	21.72	**2.69**	**2.46**	**1.28**

It can be seen from the above table that the algorithm predicted that the small ISO used in the sensor function test was within 2.7 cm horizontal and vertically which is well within the acceptable limit. Since there is no GPS integrated into the sensor, the coordinate frame origin is the geometric center of the sensor, and the depth is measured from the bottom of the sensor.

5.2 Demonstration Flight

The inverted results for one of the data sets over the large penetrator shows a clear primary polarizability curve which is like the results for a 155mm found in the library (Figure 5).

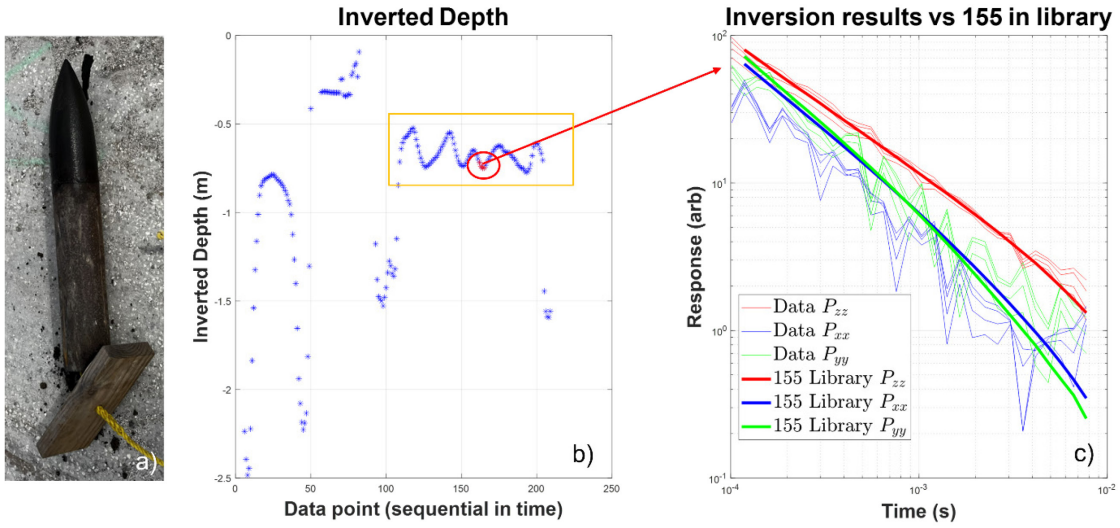

Figure 5: a) Large penetrator used as target b) Predicted depth from inversion algorithm. Yellow box indicates locations/times where the UAS was hovering, and red data points indicate the subset of data used to show polarizabilities c) resulting polarizability curves compared to 155mm found in library.

The inverted results for one of the data sets over the 81mm projectile again, shows a clear primary polarizability curve and overlays the library data well, particularly in early time.

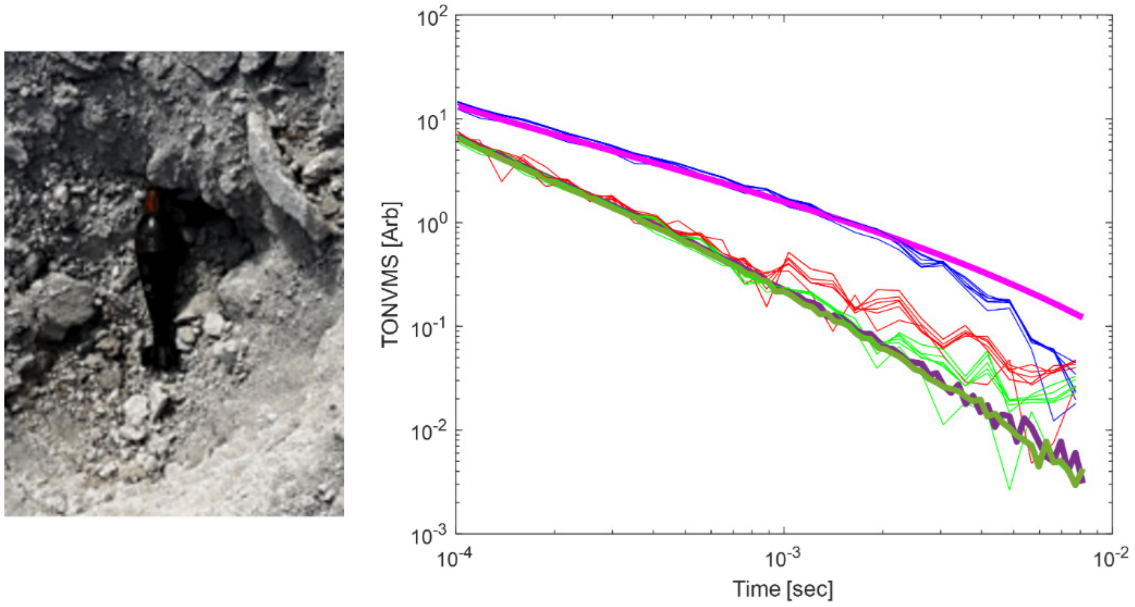

Figure 6: resulting polarizability curves compared to 82mm found in library.

6.0 DISCUSSION

As we have shown, the ULEMA-A system is capable of being deployed on a UAS system. It collects high quality data, which in return allows us to extract correct polarizabilities from a single pass of the system and classify targets as UXO and non-UXO targets. Additionally, if the GPS locations for the targets are known and are provided to the UAS, then we have also shown that the system is stable enough to transit to the waypoint and collect data. Due to the size and location of the transmitters, it is critical to have multiple transmitters and triaxial receivers. This is evident in the sensor function tests (Figure 4) which clearly shows that the primary polarizability matches the library, but the secondary and tertiary polarizabilities still appear 'jumpy'. This is likely caused from all transmitter/receiver combinations/distances which are considered when inverting the dataset. When the target is relatively small, such as the small ISO, the secondary field from the target is not strong enough to reach the receivers which are furthest from the target. This causes the weaker secondary and tertiary signals to have a smaller signal to noise ratio causing these polarizabilities to appear jumpy, particularly when target is vertical.

Additionally, neither a GPS nor a laser altimeter have yet been integrated into the sensor. The coordinates from the data inversion of the SFT shows that the inversion algorithm predict the location of the target, but without a known distance between the sensor and the ground, an accurate depth of detection cannot be extracted. Currently, all depths are reported as distance from the bottom of the sensor. In Figure 5(b), the yellow box indicates the data shots where the UAS was hovering and staying as close as possible to a single elevation. Environmental conditions such as wind and GPS accuracy cause the instability of the elevation of the UAS. It is necessary to estimate depths for both the inversions as well as obstacle avoidance during low altitude dynamic flights.

Future work on the ULEMA platforms will be focused on integrating either GPS or a laser altimeter onto the sensor and integrating the results with the EM data. This will provide accurate depths and locations of the targets referenced to the ground. We have also shown results from a simple single target environment. We know that in real-world scenarios there is usually clutter and multiple targets in an area. We will also be focusing on proving the system and the algorithms can accurately detect and classify multiple targets in real scenarios using a single pass.

7.0 CONCLUSION

A new lightweight EMI system has been built which is designed to be used either by hand or to be mounted on an unmanned vehicle, either airborne or ground based. We demonstrated the ability of the sensor to be deployed on a UAS and showed that the algorithms are designed that can correctly classify the data. The results show promise for use in more complicated environments. It should also be noted that these types of systems are usually employed to find subsurface targets, but this demonstration showed that this system may also be used to augment surface UXO detection and classification. This is of particular importance for active war zones where UXO may not penetrate the subsurface, yet is still hidden by debris making the targets indistinguishable from rubble, rocks, etc. This type of system may be used to help enhance decision making when standard, remote sensing techniques such as LiDAR and EO/IR are unable to distinguish between targets of interest.

8.0 REFERENCES

[1] Thomas Blinkhorn, "Reconstructing Ukraine: Where to Begin and When?," *1818 Quarterly* , vol. 4, no. 8, pp. 31–32, 2022.

[2] D. Etter and B. Delaney, "Report of the defense science board task force on unexploded ordnance," 2003.

[3] J. P. Fernández, B. Barrowes, K. O'Neill, I. Shamatava, F. Shubitidze, and K. Sun, "A data-derived time-domain SEA for UXO identification using the MPV sensor," in *Detection and Sensing of Mines, Explosive Objects, and Obscured Targets XIII*, 2008, vol. 6953, pp. 459–470.

[4] J. D. McNeill and M. Bosnar, "Application of TDEM techniques to metal detection and discrimination: a case history with the new Geonics EM-63 fully time-domain metal detector," *Technical Note TN-32. Missisauga, ON: Geonics LTD (http://www. geonics. com)*, vol. 8, p. 43, 2000.

[5] E. Gasperikova, J. Smith, H. F. Morrison, A. Becker, and K. Kappler, "UXO detection and identification based on intrinsic target polarizabilities—A case history," *Geophysics*, vol. 74, no. 1, pp. B1–B8, 2009.

[6] G. R. Harbaugh *et al.*, "EMI array for cued UXO discrimination," 2010.

[7] I. J. Won, D. A. Keiswetter, D. R. Hanson, E. Novikova, and T. M. Hall, "GEM-3: A monostatic broadband electromagnetic induction sensor," *J Environ Eng Geophys*, vol. 2, no. 1, pp. 53–64, 1997.

[8] K. O'Neill *et al.*, "Data diversity for UXO discrimination in realistic settings with a handheld EMI sensor," in *Detection and Remediation Technologies for Mines and Minelike Targets IX*, 2004, vol. 5415, pp. 253–262.

[9] J. P. Fernández, B. Barrowes, K. O'Neill, I. Shamatava, and F. Shubitidze, "A vector handheld frequency-domain sensor for UXO identification," in *Detection and Sensing of Mines, Explosive Objects, and Obscured Targets XIV*, 2009, vol. 7303, pp. 260–271.

[10] H. H. Nelson and J. R. McDonald, "Multisensor towed array detection system for UXO detection," *IEEE Transactions on Geoscience and Remote Sensing*, vol. 39, no. 6, pp. 1139–1145, 2001.

[11] D. D. Snyder and D. C. George, "The Advanced Ordnance Locator (AOL): A dual-mode TEM and magnetics system for detection and classification of UXO," in *Symposium on the Application of Geophysics to Engineering and Environmental Problems 2005*, 2005, pp. 1244–1253.

[12] M. Prouty, D. C. George, and D. D. Snyder, "MetalMapper: A multi-sensor TEM system for UXO detection and classification," 2011.

[13] Geometrics, "Metal Mapper 2x2," *https://www.geometrics.com/product/metalmapper-2x2/*, Feb. 28, 2023.

[14] J. P. Fernández, B. Barrowes, K. O'Neill, I. Shamatava, F. Shubitidze, and K. Sun, "A data-derived time-domain SEA for UXO identification using the MPV sensor," in *Detection and Sensing of Mines, Explosive Objects, and Obscured Targets XIII*, 2008, vol. 6953, pp. 459–470.

[15] S. Cazares, M. Tuley, and E. Ayers, "The UXO Classification Demonstration at the Former Camp Butner, NC," 2011.

[16] F. Shubitidze, G. Saparishvili, B. Barrowes, T. Shubitidze, and M. Prishvin, "ULEMA: Ultra-Light ElectroMagnetic Array system for UXO detection and classification," in *Symposium on the Application of Geophysics to Engineering and Environmental Problems 2021*, 2021, p. 21.

[17] F. Shubitidze, I. Shamatava, and A. Bijamov, "A Combined Joint Diagonalization and ONVMS Approach for ESTCP Live-Site TEMTADS Data Inversion and Classification Studies," in *Symposium on the Application of Geophysics to Engineering and Environmental Problems 2011*, 2011, p. 414.

[18] F. Shubitidze, B. Barrowes, I. Shamatava, J. P. Fernández, and K. O'Neill, "The ortho normalized volume magnetic source technique applied to live-site uxo data: Inversion and classification studies," in *SEG Technical Program Expanded Abstracts 2011*, Society of Exploration Geophysicists, 2011, pp. 3766–3770.

[19] F. Shubitidze *et al.*, "The orthonormalized volume magnetic source model for discrimination of unexploded ordnance," *IEEE Transactions on Geoscience and Remote Sensing*, vol. 52, no. 8, pp. 4658–4670, 2013.